OAK RIDGE NATIONAL LABORATORY LIBRARIES
3 4456 0549145 6

CENTRAL RESEARCH LIBRARY
DOCUMENT COLLECTION

NATIONAL LABORATORY
operated by
UNION CARBIDE CORPORATION
for the
U. S. ATOMIC ENERGY COMMISSION

ORNL-TM-1119

TIME SCALING IN ANALOG SIMULATION OF NUCLEAR SYSTEMS

L. Robert Beardsley
E. R. Mann

CENTRAL RESEARCH LIBRARY
DOCUMENT COLLECTION
LIBRARY LOAN COPY
DO NOT TRANSFER TO ANOTHER PERSON
If you wish someone else to see this document, send in name with document and the library will arrange a loan.

NOTICE This document contains information of a preliminary nature and was prepared primarily for internal use at the Oak Ridge National Laboratory. It is subject to revision or correction and therefore does not represent a final report.

ORNL-TM-1119

Contract No. W-7405-eng-26

INSTRUMENTATION AND CONTROLS DIVISION

TIME SCALING IN ANALOG SIMULATION OF NUCLEAR SYSTEMS

L. Robert Beardsley[1] and E. R. Mann

SEPTEMBER 1965

[1]Now at Mechanical Engineering Dept., University of Mississippi, University, Mississippi.

OAK RIDGE NATIONAL LABORATORY
Oak Ridge, Tennessee
operated by
UNION CARBIDE CORPORATION
for the
U.S. ATOMIC ENERGY COMMISSION

OAK RIDGE NATIONAL LABORATORY LIBRARIES

3 4456 0549145 6

CONTENTS

	Page
List of Figures	iv
Abstract	1
Introduction	1
Method	2
Results	7
Summary	13
Appendices	14
A. A Derivation of the Equations of Gain and Phase Shift of the Nuclear Reactor	14
B. Method of Linearization of Kinetic Equations	18
C. Sample Calculations	20
D. A Derivation of Phase Angle in a Phase Shifter	23
E. Nuclear Constants for Uranium-235	26
F. Disturbing Function Generators	27
G. Integrator Time Constants	30

FIGURE LIST

Dwg. or Photo No.	Caption	Page
Dwg. 65-7976	Fig. 1. Nonlinear Reactor Kinetics, Time Scale = 1.0.	4
Dwg. 65-7977	Fig. 2. Linearized Reactor Kinetics, Time Scale = 1.0.	5
Dwg. 65-7978	Fig. 3. Gain Characteristic of Linearized Reactor Kinetics.	8
Dwg. 65-7979	Fig. 4. Gain Deviation of Linearized Reactor Kinetics Simulation.	8
Dwg. 65-7980	Fig. 5. Phase Shift Characteristic of Linearized Reactor Kinetics.	9
Dwg. 65-7981	Fig. 6. Phase Shift Deviation of Linearized Reactor Kinetics Simulation.	9
Dwg. 65-7982	Fig. 7. Nonlinear vs. Linearized Variation in Power $(p-p_o)$.	12
Dwg. 65-7983	Fig. D-1. Phase Shifter Network.	24
Dwg. 65-7984	Fig. F-1. Disturbing Function Generator.	28
Dwg. 65-7985	Fig. G-1. Example of Integrator Variations with Time Scale.	31

TIME SCALING IN ANALOG SIMULATION OF NUCLEAR SYSTEMS

L. Robert Beardsley and E. R. Mann

ABSTRACT

Changes in the time scales of reactor simulations are studied. It is found that such scale changes permit more accurate simulation by restricting operation to those frequencies best handled by analog computer systems. Short computer runs (as from compressed time scales) are found to require more precise potentiometer settings. As part of the investigation, the inaccuracies introduced by linearizing the reactor kinetic equations are measured. These errors are found to be negligible when reactivity perturbations are restricted to values of less than 0.02%.

INTRODUCTION

Analog computer components can restrict the frequency range over which acceptable simulation of nuclear systems can be expected. Investigation of the stability of a reactor model may require the use of forcing functions with frequency components extending over many decades. Determination of the frequency response of the system for frequencies below 0.005 cps is time consuming, and because of the long time required for a measurement the leakage currents in the integrators may introduce unacceptable errors.

For frequencies above about 2 cps, servo components, such as multipliers and some readout devices, cannot follow the signal reliably. The mechanical inertia of these components proves to be the limiting factor in their frequency response characteristics. Thus, the frequency range over which the analog computer will operate reliably is limited by the characteristics of its servo components in the high frequency region and the leakage currents and amplifier instability in the low frequency region.

Between these two regions of computer unreliability lies the frequency range in which the analog simulation represents the mathematical model with high fidelity. To extend the range of reliable simulation the time scale of the computer problem can be changed so that simulation in the high and low frequency regions may be made with the computer

operating in a machine-time frequency range in which performance is reliable. It is often desirable to compress a simulation of a two-hour reactor run into a few minutes on the machine and, similarly, to expand a 0.1 sec excursion into a machine run of 10 sec or more. To change the time scale in a convenient manner, we make the change in decade intervals.

METHOD

To evaluate the technique of using variable time scales, we chose a model for which the results could be easily obtained without the use of an analog computer. This model is a "point reactor," as defined by the kinetic equations given below. The delayed neutron constants are those given for ^{235}U by Keepin[1] (see Appendix E), and the mean prompt neutron lifetime ℓ is assumed to be 100 μsec. The kinetic equations are

$$\frac{dp}{dt} = \frac{(1-\beta)k-1}{\ell} p + \sum_{i=1}^{6} \lambda_i c_i \tag{1}$$

and

$$\frac{dc_i}{dt} = \frac{k\beta_i p}{\ell} - \lambda_i c_i \tag{2-7}$$

These equations are nonlinear because both involve kp, a product of two dependent variables. To evaluate the frequency response of a model without the uncertainties due to nonlinear computing elements, the model is linearized. The linearized model is given by the equations

$$\frac{dy}{dt} = \frac{(1-\beta)p_o\delta k}{\ell} - \frac{\beta y}{\ell} + \sum_{i=1}^{6} \lambda_i x_i \tag{8}$$

---

[1]G. R. Keepin and T. F. Wimett, Nucleonics 16 (10), 86-90 (1958).

and

$$\frac{dx_i}{dt} = \frac{\beta_i y}{\ell} - \lambda_i x_i + \frac{\beta_i p_o \delta k}{\ell}, \tag{9-14}$$

where

$$y = p - p_o \text{ and } x_i = c_i - c_{io} \tag{15}$$

These equations (see Appendix B for development) represent the nonlinear model only at the quiescent point where $p = p_o$, $c_i = c_{io}$, and $k = 1$. However, the linear nuclear network can be made to simulate the nonlinear model to any accuracy that may be required in the neighborhood of p_o if the size of the neighborhood is chosen suitably small. The network resulting from the linear model has the same delayed neutron branches as the nonlinear network, the difference being only in the driving function to these branches. In the nonlinear network this driving signal is $p\delta k$, while in the linear network it is $p_o\delta k$. The disturbing function δk is assumed to be a sinusoidal variation in the multiplication factor k. This sinusoidal function is limited in this analysis to a machine-time frequency range of 0.05 to 0.5 cps to ensure that the frequency characteristics of the computer components do not affect the simulation. The input signal of the networks (Figs. 1 and 2) is the disturbing function δk, and the output signal is the variation in power, $p - p_o = y$. The frequency response of the networks can be specified in terms of gain and phase shift. The gain is $y/p_o\delta k$, or the fractional variation in power per unit change in the multiplication factor. The phase shift of the nuclear network is defined here as the angle by which the variation in power y lags the disturbing function δk.

The time scale of a network is dependent on the time constants of the time-dependent components, principally integrators and differentiators. Thus, in changing a nuclear network time scale, only the time constants of the integrators need be changed since no differentiators are used. Since the optimum decade is taken as 0.05 to 0.50 cps, frequencies in this decade are simulated in a unity time scale where

ORNL DWG. 65-7976

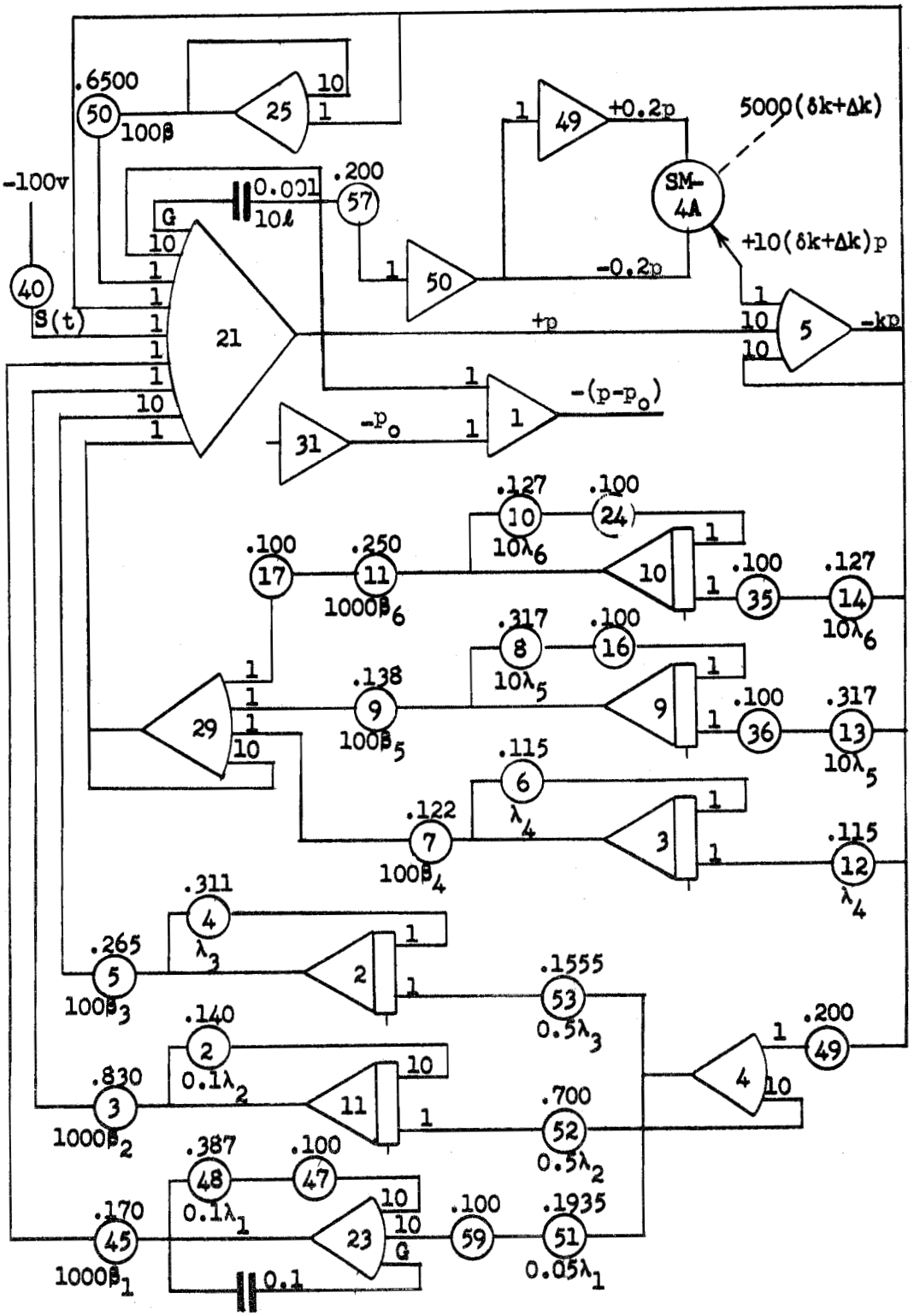

Figure 1. Nonlinear Reactor Kinetics, Time Scale = 1.0

ORNL DWG. 65-7977

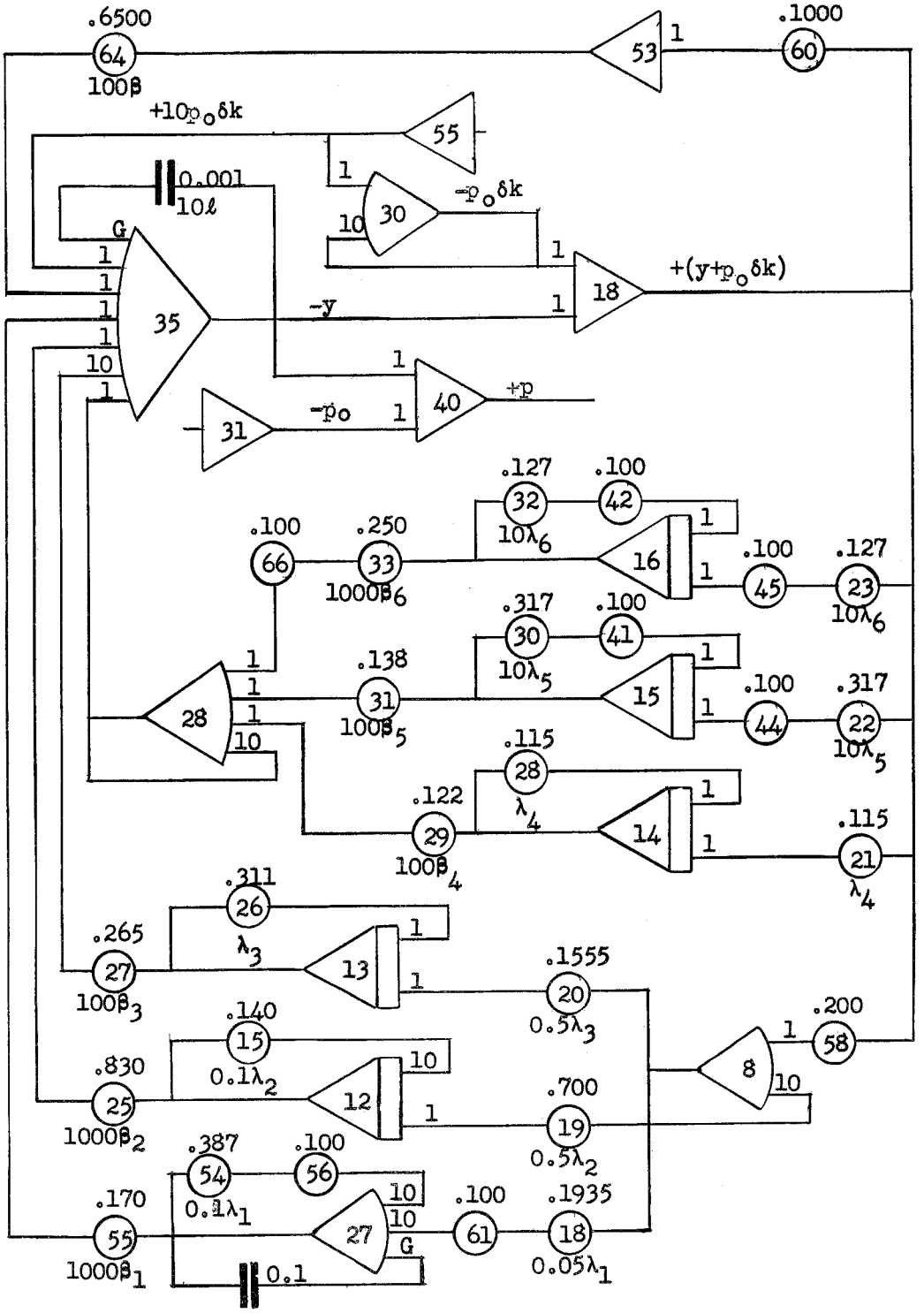

Figure 2. Linearized Reactor Kinetics, Time Scale = 1.0

machine time and prototype time are the same. The frequencies greater than 0.5 cps are simulated in time scales of 10, 100, and 1000 (machine time longer than problem time), and those frequencies below 0.05 cps are simulated in time scales of 0.1 and 0.01 (machine time shorter than problem time). This combination of time scales and frequency choice provides a six-decade range of problem frequencies from 0.0005 to 500 cps, which may be simulated by a machine time frequency range of 0.05 to 0.5 cps. To obtain these time scales, in decade intervals, the integrator time constants are varied from 100 times to 0.001 times the real-time values. The circuit configurations used in making all these changes in time constants are too numerous to discuss in complete detail, but the nuclear network for unity time scale is given in Fig. 2, and the variations in the branch which simulates the second delayed neutron group are given as a typical example in Appendix G.

The gain of the nuclear network is obtained from the ratio of the amplitudes of the two voltages y and $p_o \delta k$. The phase angle ϕ is obtained by delaying the δk voltage through a phase shifter whose delay constant is adjusted so as to match the delay through the nuclear network. With this condition satisfied, the delay constant is given by

$$\lambda = HKM/J, \tag{16}$$

where H, K, and J are input gains in the phase shifter circuit of Fig. D-1a (Appendix D) and M is the coefficient of the potentiometer. The phase angle ϕ is determined from

$$\phi = \tan^{-1} \omega/\lambda. \tag{17}$$

The derivation of these equations is given in Appendix D.

A Lissajou pattern showing the variable y as a function of delayed δk was obtained by means of a Variplotter. The nuclear delay constant was taken to be that value of delay which gave the same shaped curve for y vs delayed δk as was obtained for y vs y. The characteristics of the plotter were such that this pattern was not a single straight line but rather a pair of straight, parallel lines approximately 3/32 in. apart with small curves to close the ends.

Normally a Lissajou pattern shows that two variables such as y and the phase shifter output are in phase or 180° out of phase when the pattern is a straight line. The two parallel line configuration caused by some eccentricity of the Variplotter apparently was equivalent to the straight line configuration one normally expects when the two variables are in phase.

RESULTS

The frequency characteristics of the linear network were compared with those of the nonlinear network. The linear network data showing experimental gain and phase shift are plotted in Figs. 3 and 5 respectively, and the deviation of the experimental data from the analytic calculations are plotted in Fig. 4 and 6. The experimental data and analytic values are tabulated in Table 1. The analytic values were obtained from equations

$$\tan \phi = \frac{\dfrac{1 - \beta + A}{\beta - A} + \dfrac{C}{\ell\omega + C}}{\dfrac{1 - \beta + A}{\ell\omega + c} - \dfrac{C}{\beta - A}} \tag{18}$$

and

$$\left|\frac{y}{P_o \delta k}\right| = \frac{y_o}{p_o \Delta} = \frac{1 - \beta + A}{\ell\omega + C} \sin \phi - \frac{C}{\ell\omega + C} \cos \phi, \tag{19}$$

which are derived in Appendix A. The deviations of the experimental results from the corresponding analytic values, Figs. 4 and 6 and Table I, are generally less than 0.20 db for gain, with extremes of +0.43 and −0.47 db. The phase angle deviation was generally less than 0.3°, with extremes of +1.13° and −0.50°. The deviations at the lowest frequency point of 0.0005 cps are −0.16 db and −0.05°. To achieve these particularly small deviations the amplifiers were rechecked for null, the potentiometer settings were rechecked, and if necessary, adjusted just before data were taken for each frequency in a given decade. The time scale was 0.01. The measured quantities at 0.05 cps contained

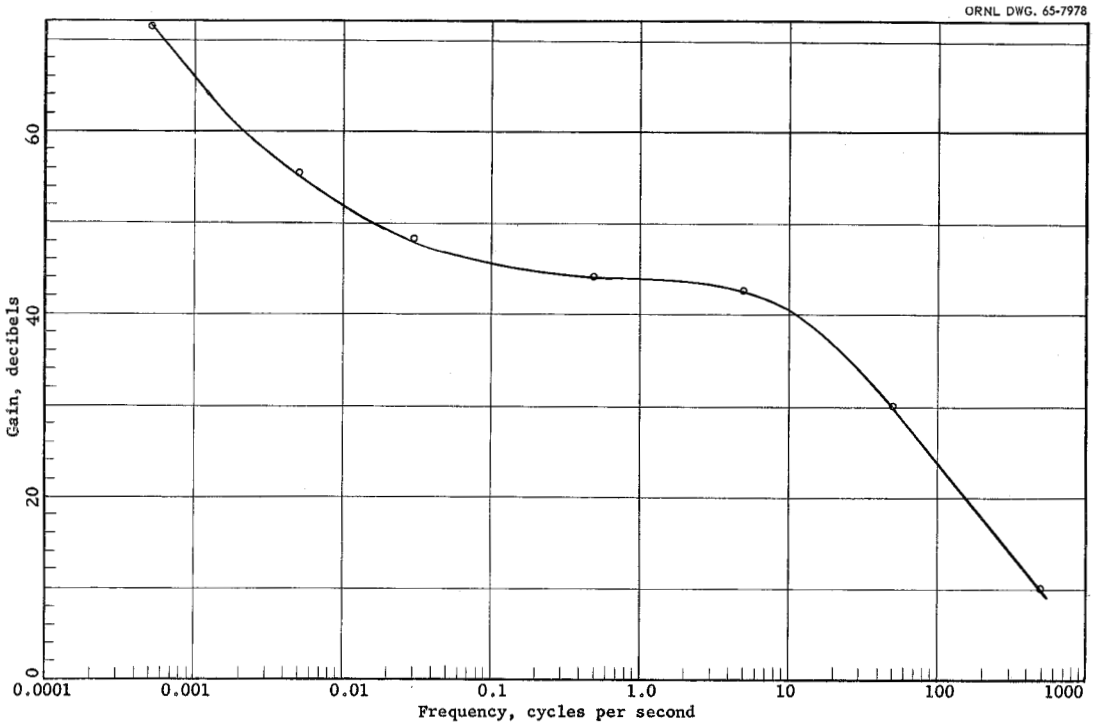

Figure 3. Gain Characteristic of Linearized Reactor Kinetics.

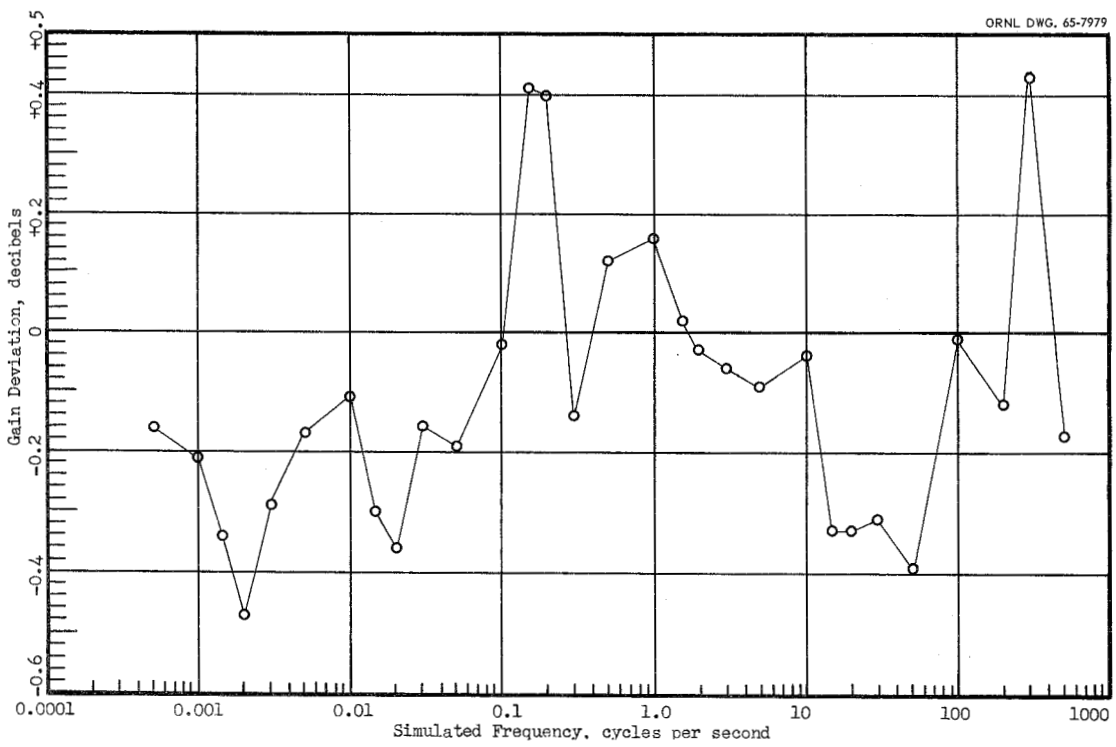

Figure 4. Gain Deviation of Linearized Reactor Kinetics Simulation.

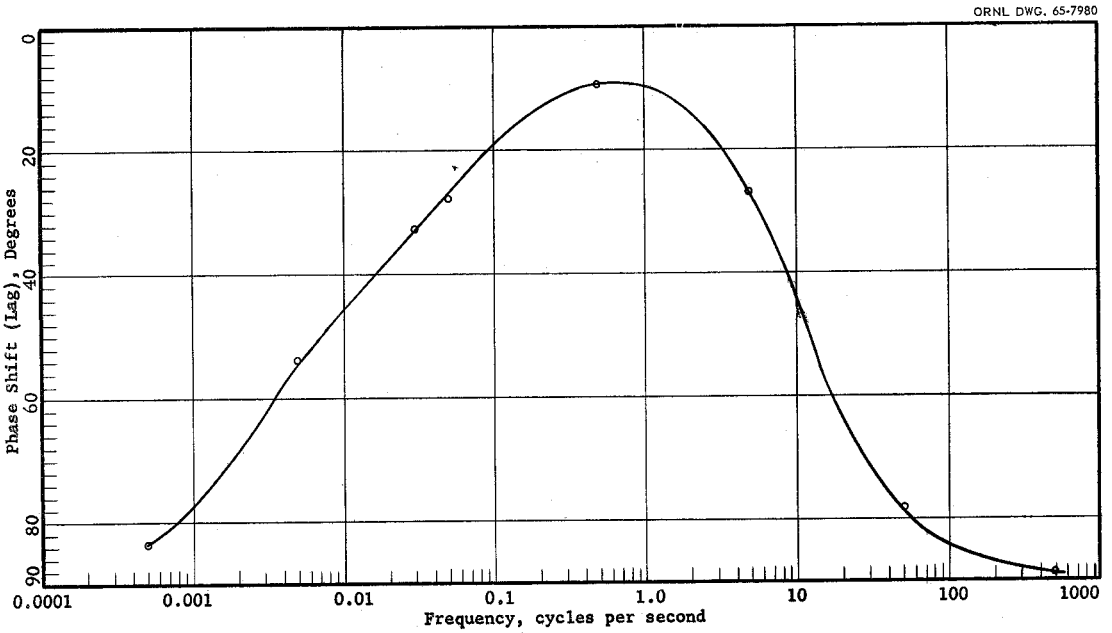

Figure 5. Phase Shift Characteristic of Linearized Reactor Kinetics.

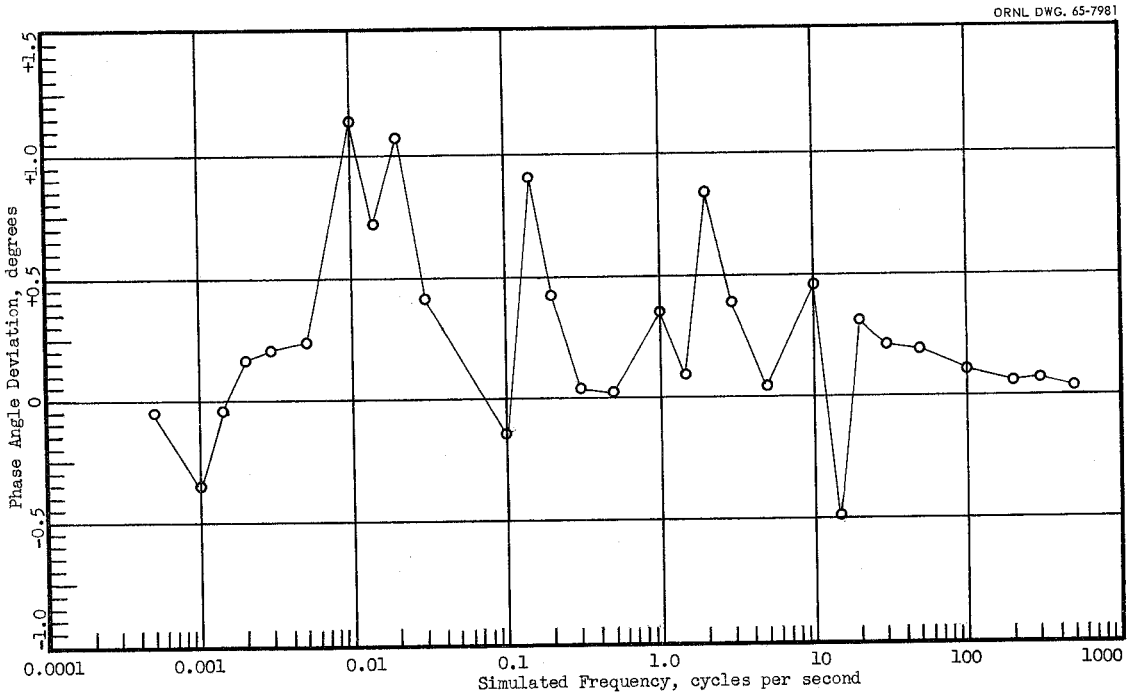

Figure 6. Phase Shift Deviation of Linearized Reactor Kinetics Simulation.

TABLE I

GAIN AND PHASE LAG OF POINT REACTOR KINETICS

Simulated Frequency cps	Gain, Decibels			Phase Lag, Degrees		
	Analog	Analytic	Deviation	Analog	Analytic	Deviation
0.0005	71.62	71.78	- .16	83.5	83.55	- .05
0.0010	65.83	66.04	- .21	77.4	77.75	- .35
0.0015	62.57	62.91	- .34	72.8	72.84	- .04
0.0020	60.37	60.84	- .47	68.9	68.74	+ .16
0.0030	57.89	58.18	- .29	62.5	62.30	+ .20
0.0050	55.18	55.35	- .17	54.0	53.77	+ .23
0.0100	52.25	52.36	- .11	45.4	44.27	+ 1.13
0.0150	50.50	50.80	- .30	40.9	40.18	+ .72
0.0200	49.37	49.73	- .36	38.5	37.43	+ 1.07
0.0300	48.14	48.30	- .16	33.7	33.29	+ .41
0.0500	46.57	46.76	- .19	15.2	27.29	- 12.09
0.100	45.34	45.36	- .02	18.9	19.05	- .15
0.150	45.26	44.85	+ .41	16.3	15.40	+ .90
0.200	44.96	44.56	+ .40	13.8	13.38	+ .42
0.300	44.09	44.23	- .14	11.2	11.17	+ .03
0.500	44.06	43.94	+ .12	9.4	9.8	+ .02
1.00	43.86	43.70	+ .16	9.6	9.25	+ .35
1.50	43.61	43.59	+ .02	11.9	10.81	+ .09
2.00	43.47	43.50	- .03	13.7	12.86	+ .84
3.00	43.23	43.29	- .06	18.8	17.41	+ .39
5.0	42.64	42.73	- .09	26.5	26.45	+ .05
10.0	40.75	40.79	- .04	44.7	44.24	+ .46
15.0	38.42	38.75	- .33	55.0	55.50	- .50
20.0	36.59	36.92	- .33	63.0	62.69	+ .31
30.0	33.63	33.94	- .31	71.2	70.99	+ .21
50	29.43	29.82	- .39	78.5	78.31	+ .19
100	23.92	23.93	- .01	84.2	84.09	+ .11
200	17.83	17.95	- .12	87.1	87.04	+ .06
300	13.86	14.43	+ .43	88.1	88.03	+ .07
500	9.83	10.00	- .17	88.85	88.81	+ .04

large errors probably because errors were made in setting the frequency of the disturbing function. These data were discarded because of the large error of -12.09°.

As in a real reactor, stability is measured by the rate of random increase or decrease in the power. This rate of change may be made extremely small, and the reactor is then said to be stable. However, if no control devices are in operation, the power may continually increase or decrease at a rate sufficiently small so as not to be detected until the normal observation time intervals are lengthened by factors of 10 or 100. This same situation exists in the analog simulations. Finding the quiescent power p_o constant for several minutes does not mean that there will be no upward or downward trend in periods of 10 or 100 times as long. To obtain stability over these longer periods, the simulation must be set up so that the prompt multiplication factor is precisely $1 - \beta$, where β is taken to be the sum of the six delay fractions $\Sigma\beta_i$.

The low frequency drift described above is in part due to the magnitude of the ratio $\frac{y}{p_o \delta k}$ which is the gain of the system. Since this ratio is higher for the low frequencies, Fig. 3, than for the high frequencies, the computer coefficients must be set with greater accuracy for measurements made in the low frequency range. Time scaling merely allows the measurements to be made more quickly and thus prevents inaccuracies due to inherent computer component drift.

The instantaneous power perturbation of the nonlinear model is compared with that of the linear model in the Lissajous patterns of Fig. 7. The scales for these curves, with the zeros as shown, were obtained by subtracting the quiescent power p_o from each instantanous power p. The nearly linear 45° pattern for $\delta k = 0.020\%$ indicates that for this input there is almost no difference in the values of power obtained from the two networks. In contrast, the patterns for larger disturbing functions indicate a nonlinear network error which increases as δk becomes larger. When δk is 0.112%, the ratio of the rate of increase of power in the nonlinear network to that in the linear network varies from approximately 1/8 to 8, in comparison with only a few percent

ORNL DWG. 65-7982

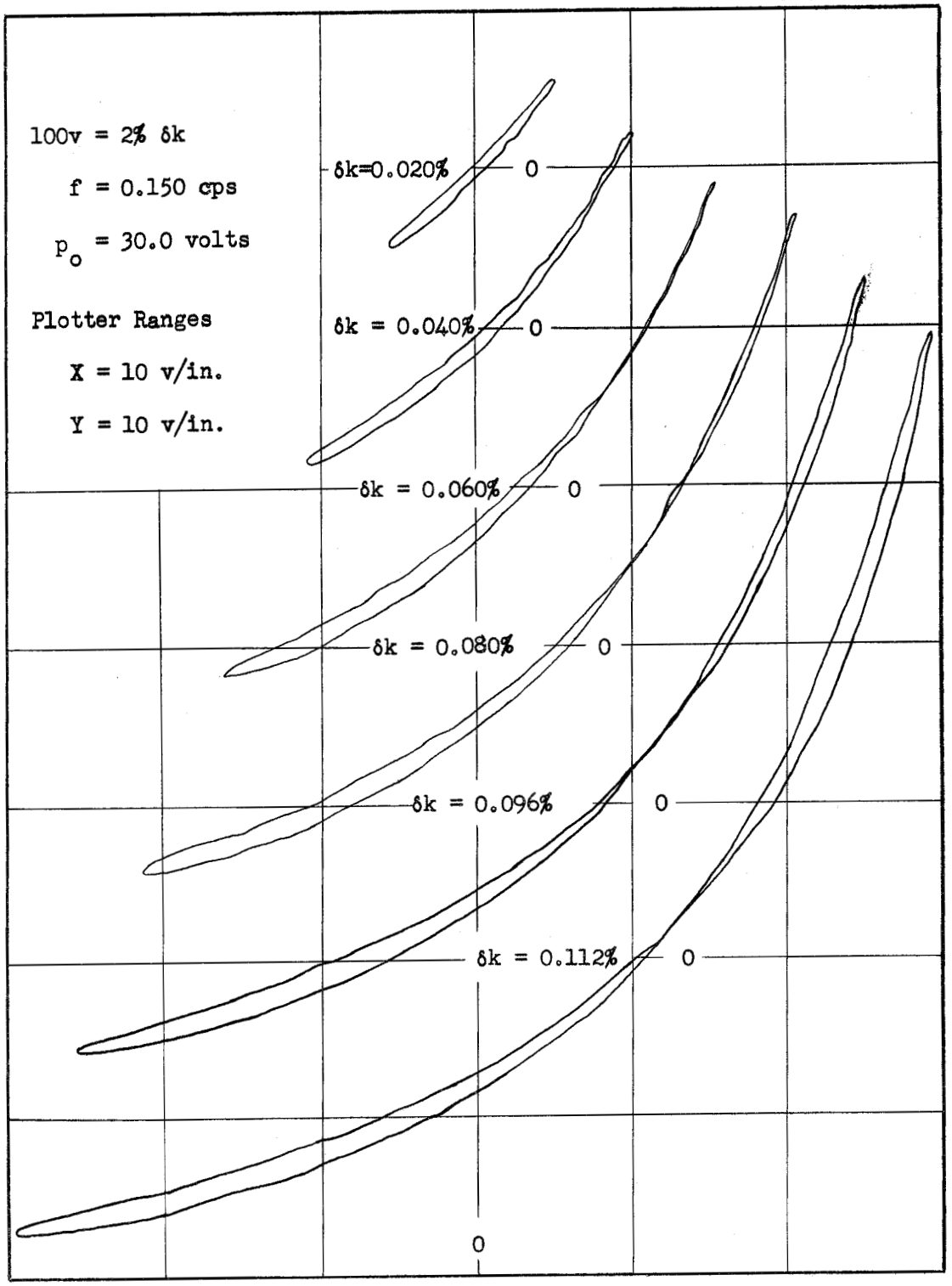

Figure 7. Nonlinear vs. Linearized Variation in Power $(p-p_o)$.

deviation from unity for $\delta k = 0.02\%$. This comparison indicates that the linear network reliably represents the nonlinear model for $\delta k < 0.02\%$, and is compatible with our assumption (Appendix B) that $\delta k \ll \beta$, where $\beta = 0.65\%$.

SUMMARY

The problem of extending the useful frequency range of the analog computer in solving nuclear reactor problems has been attacked by scaling time in the nuclear network to permit operation in the machine-time frequency range most favorable to the analog components. The experimental results show that, for the smaller compressed-time scales, the precision of certain coefficients must be increased to satisfy the requirement that, with no disturbing function, $\Sigma\beta_i = \beta$ and $k = 1$.

The random values obtained in the deviation of experimental from theoretical results indicate that the errors are not related to the the simulated, or problem, frequency or to the time scale. The ranges of the deviations are from +0.43 to −0.47 db and from +1.13 to −0.50 deg. These small errors in the gain and phase shift indicate that the simulation represents the linear model with acceptable fidelity over a frequency range of six decades. In the comparison of the nonlinear with the linear network response for values of $\delta k \ll \beta$, the differences are too small to observe.

APPENDICES

A. A DERIVATION OF THE EQUATIONS OF GAIN AND PHASE SHIFT OF THE NUCLEAR REACTOR

Beginning with the integrator of a delayed neutron group, the simplified circuit is

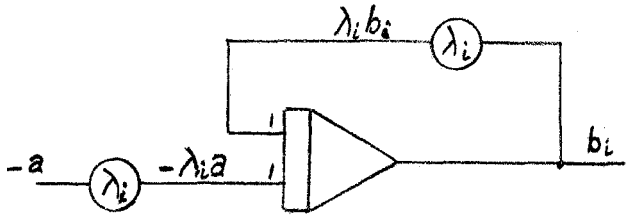

where λ_i is the delay constant. The differential equation of this circuit of the ith group is

$$-db_i/dt = -\lambda_i a + \lambda_i b_i$$

$$db_i/dt + \lambda_i b_i = \lambda_i a = \lambda_i \cos \omega t \qquad \text{(A1)}$$

where it is assumed that "a" is a unit sinusoidal function

$$a = (1) \cos \omega t \qquad \text{(A2)}$$

Then b_i must be of the form

$$b_i = A_i \cos \omega t + C_i \sin \omega t \qquad \text{(A3)}$$

where the constants A_i and C_i are to be determined. The time derivative of this equation is

$$db_i/dt = -\omega A_i \sin \omega t + \omega C_i \cos \omega t \qquad \text{(A4)}$$

Substituting Eqs. A2, A3 and A4 into Eq. A1 results in the equation

$$-\omega A_i \sin \omega t + \omega C_i \cos \omega t + \lambda_i A_i \cos \omega t + \lambda_i C_i \sin \omega t = \lambda_i \cos \omega t$$

Equating cosine terms and eliminating cos ωt gives the equation

$$\omega C_i + \lambda_i A_i = \lambda_i \tag{A5}$$

Then equating sine terms and eliminating sin ωt gives

$$-\omega A_i + \lambda_i C_i = 0 \tag{A6}$$

Solving Eqs. A5 and A6 simultaneously for A_i and C_i results in

$$A_i = \lambda_i^2/(\omega^2 + \lambda_i^2) \tag{A7}$$

$$C_i = \lambda_i \omega/(\omega^2 + \lambda_i^2) \tag{A8}$$

Substituting Eqs. A7 and A8 into Eq. A3 gives

$$b_i = \frac{\lambda_i^2}{\omega^2 + \lambda_i^2} \cos \omega t + \frac{\lambda_i \omega}{\omega^2 + \lambda_i^2} \sin \omega t$$

This is the output of the integrator. In the network of Fig. 2, the voltage fed to integrator 35 from this circuit is $(y + p_o \delta k)\beta_i b_i$ (and the powers of 10 to keep the scales correct). The total feedback from all delayed neutron groups to integrator 35 is

$$(y + p_o \delta k)\ \Sigma\beta_i b_i = (y + p_o \delta k)\ [\Sigma\beta_i A_i \cos \omega t + \Sigma\beta_i C_i \sin \omega t]$$

For simplicity in the remainder of this derivation, it is assumed that

$$A = \Sigma\beta_i A_i \tag{A9}$$

and

$$C = \Sigma\beta_i C_i \tag{A10}$$

Then

$$\Sigma\beta_i b_i = A \cos \omega t + C \sin \omega t \tag{A11}$$

Equation A11 represents the total delayed neutron rate with a unit input signal--(1) cos ωt.

The linearized equations (8-14) are multiplied by ℓ and rearranged and are given here for convenience:

$$\ell\ dy/dt = -\beta\ (y + p_o\delta k) + p_o\delta k + \Sigma\ell\lambda_i x_i$$

$$\ell\ dx_i/dt = \beta_i(y + p_o\delta k)\ -\ell\lambda_i x_i$$

The variables y and δk are assumed to be

$$y = y_o \cos \omega t \tag{A12}$$

$$\delta k = \Delta \cos\ (\omega t + \phi) \tag{A13}$$

where ϕ is the phase angle by which δk leads y. Then

$$dy/dt = -\omega y_o \sin \omega t \tag{A14}$$

When these functions are substituted for their variables in the first linearized kinetic equation, it takes the form

$$-\ell\omega y_o \sin \omega t = \beta[y_o \cos \omega t + p_o\Delta \cos\ (\omega t + \phi)\ ]$$
$$+p_o\Delta \cos\ (\omega t + \phi) + \Sigma\ell\lambda_i x_i \tag{A15}$$

From Fig. 2, again it will be noted that the driving function to the delayed neutron group circuits is $(y + p_o\ \delta k)$ instead of the unit function given in Eq. A2.

The last term of Eq. A15 then becomes, for the ith group,

$$\ell\lambda_i x_i = \beta_i b_i\ (y + p_o\delta k)$$

and

$$\Sigma\ell\lambda_i x_i = [\Sigma\beta_i A_i \cos \omega t + \Sigma\beta_i C_i \sin \omega t]\ (y + p_o\ \delta k) \tag{A16}$$

Now, if Eq. A15 is written in phasor notation, cos ωt is replaced by (1), unity, and sin ωt is replaced by (-j) and the equation becomes

$$j\ell\omega y_o = -\beta(y_o + p_o\Delta \cos\phi + jp_o\Delta \sin\phi) + p_o\Delta \cos\phi$$

$$+ jp_o\Delta \sin\phi + (y_o + p_o\Delta \cos\phi + jp_o \Delta \sin\phi)\ (A-jC) \qquad \text{(A17)}$$

Collecting the imaginary terms and simplifying yields

$$\ell\omega y_o = -\beta p_o\Delta \sin\phi + p_o\Delta \sin\phi + A\ p_o\Delta \sin\phi - C(y_o + p_o\Delta \cos\phi)$$

$$= p_o\Delta \sin\phi\ (-\beta + 1 + A)\ -Cy_o\ -C\ p_o \cos\phi$$

$$(\ell\omega + C)\ y_o = p_o\Delta\ (1 - \beta + A)\ \sin\phi - C\ P_o\Delta \cos\phi \qquad \text{(A18)}$$

The real terms now simplify to give

$$0 = -\beta(y_o + p_o\Delta \cos\phi) + p_o\Delta \cos\phi$$

$$+ (y_o + p_o\Delta \cos\phi)\ A + C\ p_o\Delta \sin\phi$$

This reduces to

$$y_o(\beta-A)/(p_o\Delta) = (1-\beta+A)\ \cos\phi\ C \sin\phi \qquad \text{(A19)}$$

The two variables in Eqs. A18 and A19 are gain $[y_o/(p_o\Delta)]$ and the phase angle ϕ. The simultaneous solution of Eqs. A18 and A19 yields

$$\tan\phi = \frac{\dfrac{1-\beta+A}{\beta-A} + \dfrac{C}{\ell\omega+C}}{\dfrac{1-\beta+A}{\ell\omega+C} - \dfrac{C}{\beta-A}} \qquad \text{(A20)}$$

and for the gain in terms of ϕ is

$$\frac{y_o}{p_o\Delta} = \frac{1-\beta+A}{\ell\omega+C} \sin\phi - \frac{C}{\ell\omega+C} \cos\phi. \qquad \text{(A21)}$$

These last two equations are carried to the text as Eqs. 18 and 19.

B. METHOD OF LINEARIZATION OF KINETIC EQUATIONS

The nonlinear equations of reactor kinetics (1 and 2-7) are repeated here for reference

$$\frac{dp}{dt} = \frac{(1-\beta)k-1}{\ell} p + \sum_{i=1}^{6} \lambda_i c_i$$

and

$$\frac{dc_i}{dt} = \frac{k\beta_i p}{\ell} - \lambda_i c_i$$

When the variables p, c_i and k are p_o, c_{io} and unity respectively, a quiescent condition is obtained. Using the quiescent values, these equations become

$$\frac{dp_o}{dt} = \frac{(1-\beta) - 1}{\ell} p_o + \sum_{i=1}^{6} \lambda_i c_{io}$$

and

$$\frac{dc_{io}}{dt} = \frac{\beta_i p_o}{\ell} - \lambda_i c_{io}$$

Subtracting the second set from the first set of equations, the result is

$$\frac{d(p-p_o)}{dt} = \frac{(1-\beta) - 1}{\ell} (p-p_o) + \frac{(1-\beta)\delta k(p-p_o)}{\ell} + \frac{(1-\beta)p_o\delta k}{\ell} + \sum_{i=1}^{6} \lambda_i (c_i - c_{io})$$

and

$$\frac{d(c_i-c_{io})}{dt} = \frac{\beta_i(p-p_o)}{\ell} + \frac{\beta_i \delta k(p-p_o)}{\ell} + \frac{\beta_i p_o \delta k}{\ell} - \lambda_i (c_i - c_{io})$$

It is then assumed that

$$|p-p_o| < \Delta_i, |c_i - c_{io}| < \Delta_2 \text{ and } |\delta k| < \Delta_3$$

that Δ_i is some small positive number, and that $\delta k \ll \beta$.

Now let $y = p-p_o$ and $x_i = c_i - c_{io}$ and rewrite the last two equations as follows:

$$\frac{dy}{dt} = \frac{(1-\beta)p_o\delta k}{\ell} - \frac{\beta y}{\ell} + \sum_{i=1}^{6}\lambda_i x_i$$

$$\frac{dx_i}{dt} = \frac{\beta_i y}{\ell} - \lambda_i x_i + \frac{\beta_i p_o \delta k}{\ell}$$

neglecting terms having the product $\delta k(p-p_o)$. Note that the term with $\beta(p-p_o)$ is retained, so that the development is valid only for $\delta k \ll \beta$.

C. SAMPLE CALCULATIONS

The gain and phase shift are calculated for the frequency of 0.0005 cps. The gain of the network is $y/p_o \delta k$ where $y = p-p_o$. The experimental data for this point show the simulation quantities to be

$$y = 45.7 \text{ volts}$$

$$p_o = 30.0 \text{ volts}$$

$$\delta k = 0.1 \times 20v = 2.0 \text{ volts}$$

The scale factors of y and p_o are the same in the network considerations, but no value has been established. These identical scale factors cancel in the gain equation. However, the scale factor for the disturbance function δk is 100 volts/2 per cent. Substitution of these values and scale factor into the gain equation gives

$$\frac{y}{p_o \delta k} = \frac{45.7}{30 \times 2.0\ (0.02/100)} = 3810$$

In order to obtain a reasonable scale for the total range of gain from 3.10 to 3810, a decibel scale was chosen. This scale is linear while representing a logarithmic scale of gain. The gain in decibels is then

$$\text{gain(db)} = 20 \log_{10} 3810 = 71.62 \text{ db}$$

The phase shift is given by Eq. 17 as

$$\phi = \tan^{-1} \omega/\lambda$$

where ω is the frequency in radians per second and λ is the delay constant for the phase shifter network of Fig. D-1. The data for this portion of the frequency response of the network are

$$\lambda = HKM/J = 1\ (10)\ 0.036/10 = 0.036 \text{ sec}^{-1} .$$

In order to avoid the scaling of time in the phase shifter network, the calculations are based on the real-time frequency of the sine-wave generator. For this consideration the frequency is 0.05 cps or 0.31416 radians per second. The equation of the phase angle is then

$$\tan \phi = 0.31416/0.036 = 8.73$$

and the angle by which the output of the phase shifter lags the input is

$$\phi = 83.5 \text{ degrees}$$

The analytic solution for the same point (0.0005 cps) is obtained from the equations which are derived in Appendix A, and are

$$\tan \phi = \frac{\dfrac{1-\beta+A}{\beta-A} + \dfrac{C}{\ell\omega+C}}{\dfrac{1-\beta+A}{\ell\omega+C} - \dfrac{C}{\beta-A}} \tag{18}$$

$$\frac{y_o}{p_o\Delta} = \frac{1-\beta+A}{\ell\omega+C} \sin \phi - \frac{C}{\ell\omega+C} \cos \phi \tag{19}$$

In this work, the mean neutron lifetime, ℓ, is taken as 10^{-4} seconds. The total delay fraction is 0.0065 and the frequency being considered is 0.0031416 radians per second (0.0005 cps). The remaining constants, A and C, are those defined by equations

$$A = \sum_{i=1}^{6} \beta_i A_i \tag{A9}$$

and

$$C = \sum_{i=1}^{6} \beta_i C_i \tag{A10}$$

where A_i and C_i are given by

$$A_i = \lambda_i^2/(\omega^2 + \lambda_i^2) \tag{A7}$$

and

$$C_i = \lambda_i\omega/(\omega^2 + \lambda_i^2) \tag{A8}$$

The values of β_i and λ_i, from the table in Appendix E, together with the values of ℓ, β and ω were entered as data in a digital computer program containing equations A9, A10, A7, A8, 18 and 19. The analytic

values of Table I were obtained from this program for all the frequencies indicated. For the frequency considered here (0.0005 cps), the phase angle is

$$\phi = 83.5491 \text{ degrees}$$

and

$$\text{Gain} = y_o/p_o\Delta = 3879.87$$

which in decibels is

$$20 \log_{10} 3879.87 = 71.78 \text{ decibels}$$

The deviation in experimental gain then is

$$\text{dev.} = \text{exp.} - \text{analytic}$$

$$= 71.62 - 71.78 = -0.16 \text{ db}$$

The deviation in phase shift is

$$\Delta\phi = \text{exp.} - \text{analytic}$$

$$= 83.5^\circ - 83.55^\circ$$

$$= -0.05 \text{ degrees}$$

D. A DERIVATION OF PHASE ANGLE IN A PHASE SHIFTER

In order to determine the phase lag in the simplified network of Fig. D-1 (b) where the amplifier gains are all unity, consider the input voltage a and the output voltage b. Then the input to integrator 17 is given by

$$-db/dt = \lambda a + \lambda b$$

Rewriting to eliminate negative signs gives the equation

$$db/dt + \lambda b = \lambda a \qquad \text{D1}$$

Now if the input voltage is sinusoidal and of the form

$$a = (1) \cos \omega t \qquad \text{D2}$$

the output voltage b is a sinusoidal function

$$b = A \cos \omega t + C \sin \omega t \qquad \text{D3}$$

where the values of A and C are to be determined. Then

$$db/dt = - \omega A \sin \omega t + \omega C \cos \omega t \qquad \text{D4}$$

Substitution of Eqs. D2, D3 and D4 into Eq. D1 gives

$$-\omega A \sin \omega t + \omega C \cos \omega t + \lambda A \cos \omega t + \lambda C \sin \omega t = \lambda \cos \omega t. \qquad \text{D5}$$

Equating sine terms and eliminating sin ωt yields

$$-\omega A + \lambda C = 0$$

Then

$$A = C\lambda/\omega \qquad \text{D6}$$

Now equating cosine terms and eliminating cos ωt from both sides gives

$$\omega C + \lambda A = \lambda \qquad \text{D7}$$

The substitution of Eq. D6 into Eq. D7 yields the equation

$$C = \lambda\omega/(\omega^2 + \lambda^2) \qquad \text{D8}$$

ORNL DWG. 65-7983

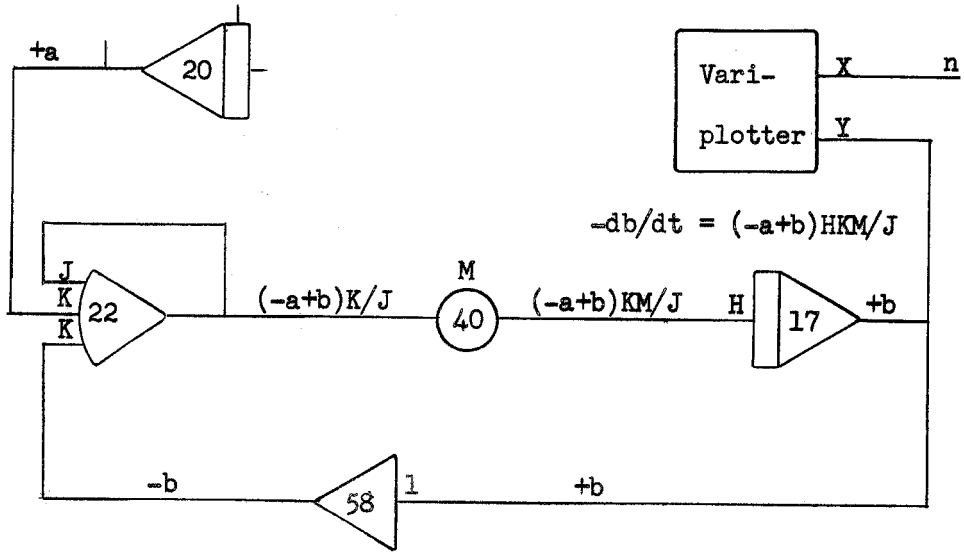

(a) Actual Circuit.

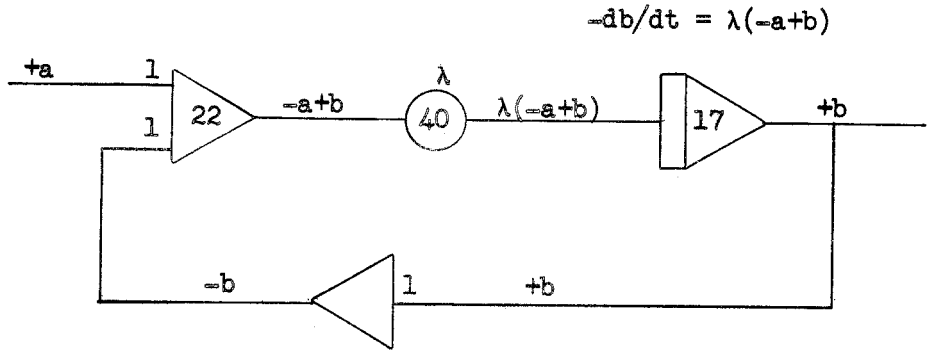

(b) Simplified Circuit.

Figure D-1. Phase Shifter Network.

Substituting this into Eq. D6 results in

$$A = \lambda^2/(\omega^2 + \lambda^2) \qquad \text{D9}$$

As an alternate to Eq. D3, the output, b, may be given by

$$d = D \cos (\omega t - \phi)$$

where the angle of lag, ϕ, is given by

$$\phi = \tan^{-1} (C/A) = \tan^{-1} \omega/\lambda$$

and the gain, D, is determined from the coefficients of Eq. D3 by the equation

$$D = (A^2 + C^2)^{0.5} = \lambda/(\omega^2 + \lambda^2)^{0.5}$$

Because the required range of phase shift requires values of λ from about 0.01 to 100 seconds^{-1}, additional gain is required. This gain can be obtained only from the amplifiers. In the actual phase shifter circuit of Fig. D-1(a), the amplifier gains are H, J and K and the coefficient of potentiometer 40 is M. Thus, by adjusting the gains as well as the coefficient, the delay constant λ may be made to vary over four decades with accuracies to at least the third significant figure. The total gain (over the 4-decade range from 0.01 to 100) is then given by the equation

$$\lambda = HKM/J$$

where H, K and J may have the precise values of unity or ten.

E. NUCLEAR CONSTANTS FOR URANIUM-235

The values of delay fractions and decay constants for the several groups of delayed neutrons resulting from fissioning of uranium-235, and which were used in this work, are given in the following Table.

TABLE E

NUCLEAR CONSTANTS FOR URANIUM-235

Group	Decay Constant Sec^{-1}	Delay Fraction rounded to 5 places
1	0.0127	.00025
2	0.0317	.00138
3	0.115	.00122
4	0.311	.00265
5	1.40	.00083
6	3.87	.00017
		.006500

F. DISTURBING FUNCTION GENERATORS

The disturbing function generator used to drive the linear and nonlinear nuclear networks is given in Figure F-1. Since it was felt advisable to start the disturbing function generator and check the magnitude of the variation, the function switch FS-3 was used to perform the functions of reset, hold and operate for the integrators in the disturbing function generator. By this technique, it was possible to verify the amplitude stability of the disturbing function over long periods without operating the nuclear networks.

The application of the sinusoidal disturbing function δk to the nuclear networks was made through the second function switch FS-2 which applied a sinusoidal signal to summer 39. Servo multiplier SM-3B was energized by amplifiers 39 and 54 and was positioned by the magnitude of the quiescent power p_o, thus providing an output of $+10p_o\delta k$ from amplifier 55 for use in the linear network.

Due to the nonlinearity of the nonlinear network, it was necessary to introduce a direct current potential identified as Δk whose magnitude was found experimentally such that, when applied as part of disturbing function, the quiescent power p_o in the nonlinear network would be maintained constant over a period of sufficient length so as to obtain the required data. This dc potential is a function of the amplitude as well as the frequency of the disturbing function. The total disturbing function $(\delta k + \Delta k)$ is fed into the motor of servo multiplier SM-4 whose first potentiometer SM-4A has, then, for its output $+10(\delta k + \Delta k)$ in the nonlinear nuclear network.

In order to eliminate the very slight drifting due to inaccuracies in the settings of the potentiometers in the networks, the shim rod potentiometers for the nonlinear (N) and the linear (L) networks were included using potentiometers 78, 76, 77, and 68.

The frequency-determining constants of this sinusoidal source are the input resistors and the feedback capacitors of integrators 19 and 20, the coefficients of potentiometers 73 and 74 and the gains of summer 7. Since the resistance and capacitance of these components are accurate

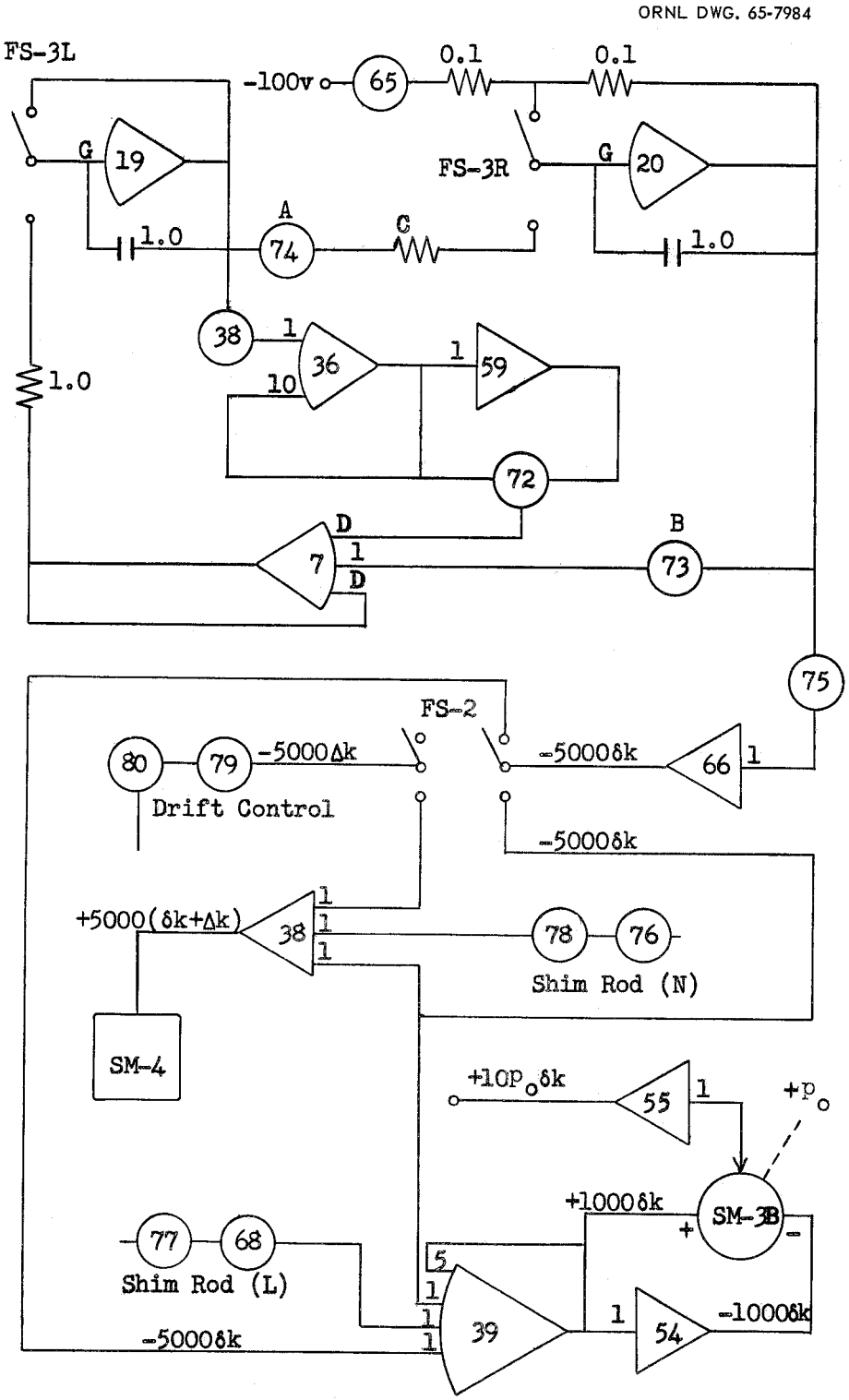

Figure F-1. Disturbing Function Generator.

to 0.01 percent when new, and the coefficients of potentiometers 73 and 74 are accurate to four places by the digital voltmeter, the frequency errors will be less than about 0.04 percent. The amplitude stability of the sinusoidal generator was found to be sufficient over a few minutes providing no feedback from the output of integrator 19 to summer 7 or the input of integrator 19 was used; however, due to inherent losses in the components of the simulation, it was necessary to provide feedback to overcome these losses. Thus, amplifiers 36 and 59 and ungrounded potentiometer 72 were included so as to provide a very critical adjustment of amplitude in controlling feedback. Potentiometer 38 in the input of amplifier 36 was set approximately 0.01 so that the signals to potentiometer 72 were extremely small. This allowed variations of nearly one-half revolution in potentiometer 72 as a range for trimming the amplitude of integrator 20 to a constant value of 20 volts over periods as long as an hour. Potentiometer 65 provided the initial condition potential of 20 volts and established the amplitude of the disturbing function generator amplitude.

G. INTEGRATOR TIME CONSTANTS

Since there are a great many network configurations possible in order to obtain the several integrator time constants necessary for changing each of the integrators for each time scale, only an example is given here. The example given is for integrator 12 which is used in the delay section of the nuclear network representing the second delay group. This section of the linear network is given in Figure G-1 for time scales from 0.01 to 100. The coefficients of potentiometers 15, 19 and 58 are given decimally with the function of the decay constant included for potentiometers 15 and 19. Time scale of the integrator is determined by potentiometers 15 and 19 while magnitude scale factors are partially controlled by the coefficients of potentiometers 19 and 58. Thus, the coefficient of potentiometer 19 combines time-scale and amplitude-scale factors. For the very fast (compressed-time) time scale of 0.01, it was found necessary to reduce the feedback capacitor in the integrator since the input resistors could not provide sufficient gain for a 1.0 microfarad capacitor. Due to the pecularities of the amplifiers available, it was necessary to replace the amplifier used for other time scales with one which could satisfactorily operate with a 0.1 microfarad feedback capacitor. This amplifier indicated as No. 25 did not have a sufficient number of high-gain input connections to serve the required purpose. The solution to this complication of hardware was obtained by using the summing junction of amplifier 12 as the summing junction for amplifier 25. This arrangement provided stable operation of amplifier 25 with a feedback capacitor of 0.1 microfarad and the high-gain inputs of amplifier 12.

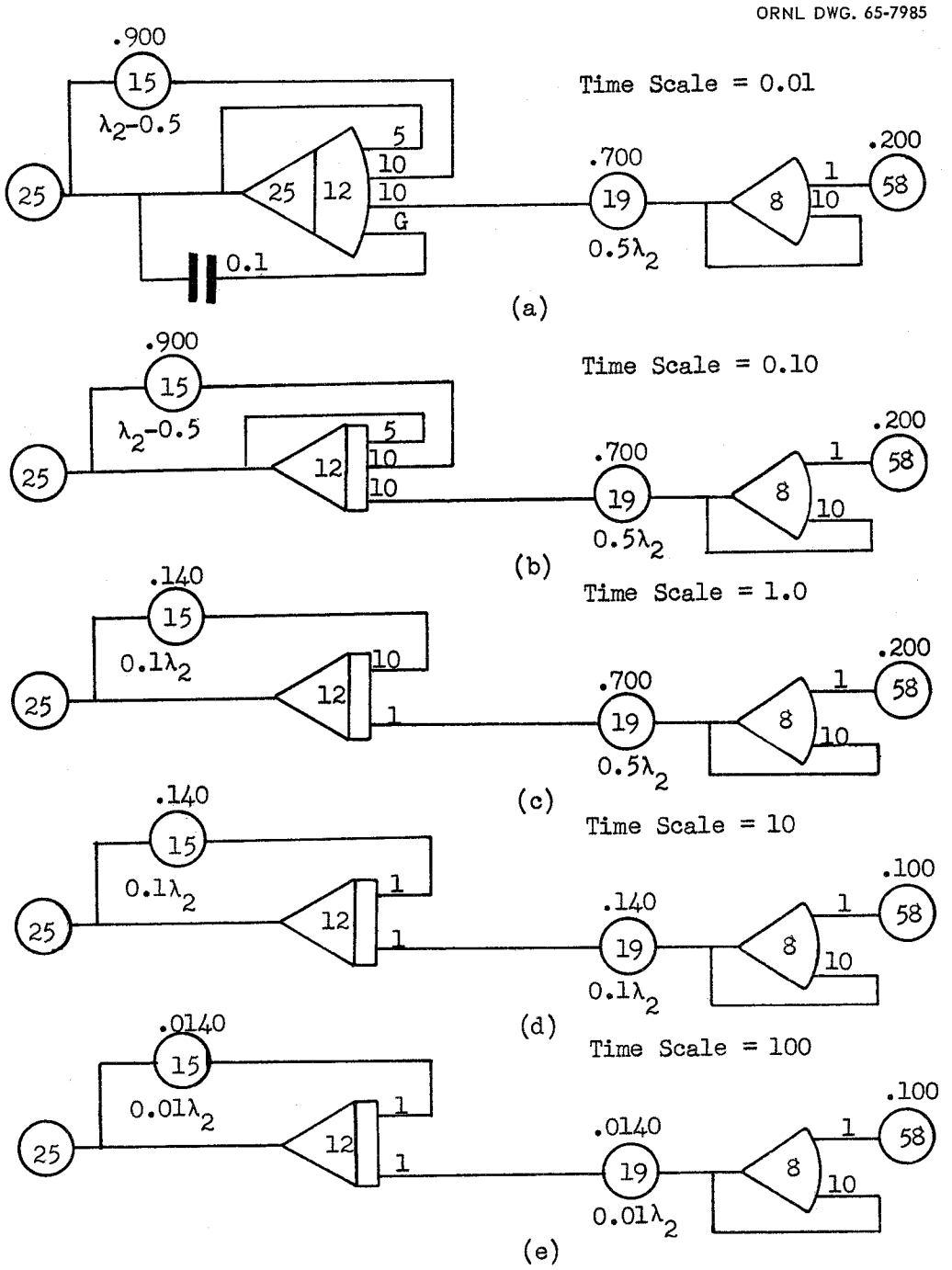

Figure G-1. Example of Integrator Variations with Time Scale.

INTERNAL DISTRIBUTION

1-2. Central Research Library
3. Document Reference Section
4-6. Laboratory Records Department
7. Laboratory Records, ORNL R.C.
8. ORNL Patent Office
9-23. Division of Technical Information Extension
24. Research and Development Division, ORO
25. S. J. Ball
26. C. J. Borkowski
27. O. W. Burke
28. S. J. Ditto
29-43. E. P. Epler
44. D. N. Fry
45. W. H. Jordan
46. B. R. Lawrence
47. L. C. Oakes
48. H. G. O'Brien
49. C. W. Ricker
50. D. P. Roux
51. R. S. Stone
52. J. R. Tallackson
53. C. S. Walker

EXTERNAL DISTRIBUTION

54-55. L. R. Beardsley, University of Mississippi, University, Mississippi
56. S. H. Hanauer, University of Tennessee, Knoxville, Tennessee